Probability of instant rail break induced by wheel–rail impact loading using field test data

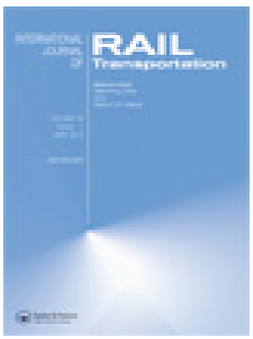

International Journal of Rail Transportation

ISSN: (Print) (Online) Journal homepage: https://www.tandfonline.com/loi/tjrt20

Probability of instant rail break induced by wheel–rail impact loading using field test data

Jens CO Nielsen , Thomas JS Abrahamsson & Anders Ekberg

To cite this article: Jens CO Nielsen , Thomas JS Abrahamsson & Anders Ekberg (2021): Probability of instant rail break induced by wheel–rail impact loading using field test data, International Journal of Rail Transportation, DOI: 10.1080/23248378.2021.1874552

To link to this article: https://doi.org/10.1080/23248378.2021.1874552

Published online: 16 Feb 2021.

INTERNATIONAL JOURNAL OF RAIL TRANSPORTATION
https://doi.org/10.1080/23248378.2021.1874552

Taylor & Francis
Taylor & Francis Group

Probability of instant rail break induced by wheel–rail impact loading using field test data

Jens CO Nielsen, Thomas JS Abrahamsson and Anders Ekberg

Department of Mechanics and Maritime Sciences, Chalmers University of Technology, Gothenburg Sweden

ABSTRACT

The probability of an instant rail break, initiated at a single pre-existing rail foot crack due to a severe wheel impact loading, is predicted using statistical methods and a time-domain model for the simulation of dynamic vehicle–track interaction. A linear elastic fracture mechanics approach is employed to calculate the stress intensity at the crack in a continuously welded rail subjected to combined bending and temperature loading. Based on long-term field measurements in a wayside wheel load detector, a three-parameter probability distribution of the dynamic wheel load is determined. For a faster numerical assessment of the probability of failure, a thin plate spline regression is implemented to develop a meta-model of the performance function quantifying the stress intensity at the crack. The methodology is demonstrated by investigating the influence of initial crack length, fracture toughness and rail temperature difference on the risk for an instant rail break.

ARTICLE HISTORY
Received 24 September 2020
Revised 7 December 2020
Accepted 7 January 2021

KEYWORDS
Wheel–rail impact loads; rail break probability; dynamic vehicle–track interaction; thin plate spline; subset simulation algorithm

1. Introduction

Wheel–rail impact loads generated by discrete wheel tread irregularities may cause severe damage of track and vehicle components leading to high maintenance costs and traffic disruptions. Common examples of such irregularities are wheel tread material fall-out due to surface damage caused by rolling contact fatigue clusters or by the wheel sliding on the rail (wheel flats) [1–3]. Monitoring of vertical dynamic wheel–rail contact forces in a wheel impact load detector provide operators with information on the current status of their wheels. To prevent unacceptable deterioration levels and safety-related failures, alarm limits are prescribed. The UIC recommended alarm limit in peak load, proclaiming an immediate stop of the train for wheel removal, is 350 kN with an alert level at 300 kN [4]. Cost-efficient and reliable railway operations require a minimum of traffic disruptions. To this end, alarm limits should provide a balance between preventing operational failures and minimizing the number of stopped trains. An understanding of the influence of wheel tread irregularities on the risk for track damage (including instant rail breaks) is the scientific basis for such optimized alarm limits.

According to a recent assessment of freight train derailments in the EU, USA and Russia [5], rail failures was ranked as one of the top eight causes. These derailments are

CONTACT Jens CO Nielsen Department of Mechanics and Maritime Sciences, Chalmers University of Technology, Gothenburg SE-412 96, Sweden jens.nielsen@chalmers.se

usually a consequence of the fracture of the rail due to high dynamic wheel loads and can be associated with internal defects that have reduced the strength of the rail section. Examples of contributing factors include high bending stresses in the rail, inadequate rail support conditions and high thermal tensile stresses.

For a given discrete wheel tread irregularity, the magnitude of the generated impact load is influenced by the three-dimensional shape of the defect and several other parameters such as train speed, axle load, and the dynamics of the coupled vehicle–track system. The parameters particularly influencing the vertical dynamics of the system are the vehicle unsprung mass and track stiffness, in particular the rail pad stiffness and ballast/subgrade stiffness at the impact position. For a given combination of tread defect and operational parameters, a maximum in impact load can be expected if the lateral position of the maximum depth of the defect is coinciding with the lateral centre of the wheel–rail contact, and the impact occurs where the track stiffness is maximum, e.g. above a sleeper on a ballasted plain line. The generated wheel–rail impact load may cause an instant rail break if it occurs near a pre-existing crack in the rail. This could lead to a train derailment, especially if the same tread damage generates multiple, adjacent rail breaks due to subsequent impacts. Wheel tread irregularities also lead to increased levels of rolling noise, impact noise and ground-borne vibration [6].

The accuracy and computational effort of various reliability assessment methods have been compared by Rahrovani et al. [7]. In their evaluation of the risk for sleeper cracking, where rail pad stiffness and ballast/subgrade stiffness were considered as stochastic variables, response surface models (meta-models) were used to approximate the performance function of the sleeper bending stress. These were generated based on different combinations of polynomial functions and sampling methods for the applied design of experiments [8]. The subset simulation algorithm proposed by Au and Beck [9] was used in the probabilistic failure analysis to determine sleeper support conditions that increase the risk of sleeper failure. Another review of techniques to reduce the computational effort required in design optimization is presented in [10], where meta-models based on polynomials, splines, kriging, neural networks, etc., are discussed.

In [11], crack growth rates and the probability of rail breaks due to wheel–rail impact were studied. It was shown that rail temperature relative to the stress-free temperature has a major influence on the risk for rail breaks in a continuously welded rail. Further, for a given crack position along the rail, it was concluded that the influence of a prescribed distribution of severe impact loads on the fatigue crack growth is minor since the stochastic spread in distance between the impact position and the crack will lead to that only a few of the impacts will have a significant influence on the loading of the crack. Combinations of initial crack lengths and impact load magnitudes that may cause rail breaks were predicted in [12]. Various scenarios in terms of operational conditions and rail temperatures were studied, and an alarm limit for impact load was proposed. To reduce the number of disturbances of operating traffic to a minimum, it was concluded that a seasonal (temperature-dependent) variation in allowable wheel load limit is justified. In [13], a fracture mechanics approach was applied to study the effects of impact loads, seasonal variation in thermal stresses as well as residual stresses from manufacturing, on fatigue crack growth in rails using a finite element (FE) model. However, the influence of the stochastic spread in impact positions was neglected.

In this paper, a methodology for the prediction of the probability of the rare event of an instant rail break initiated at a given pre-existing rail foot crack due to wheel–rail impact loading will be presented. Two stochastic variables with given probability distributions are considered: the magnitude of the dynamic wheel–rail contact load induced at the impact position, and the longitudinal position of the impact relative to the position of the existing crack. To provide a realistic traffic scenario, a probability distribution of dynamic loads is derived based on long-term measurements in a wheel impact load detector, while the longitudinal impact position has a uniform distribution over a distance corresponding to the wheel circumference. It is assumed that linear elastic fracture mechanics is valid, and that normal stresses due to rail bending and temperature-induced thermal loads is the dominating mode of loading [11,12]. The methodology is demonstrated for a case with a single, pre-existing rail foot crack. Such cracks typically initiate at corrosion pits or due to poor handling of the rail during track construction. The influences of initial crack length, rail temperature difference and fracture toughness are considered in a subsequent parameter study.

2. Wheel impact load detector data

Malmbanan is a single-track railway line in the northern part of Sweden. Traffic is dominated by iron ore freight trains with nominal axle loads 30 tonnes (speed 60 km/h) and other freight trains with axle loads up to 25 tonnes (speeds up to 120 km/h). This traffic load in combination with severe weather conditions (cold winters and relatively warm summers) put tremendous strains on the infrastructure and rolling stock.

Several wheel impact load detectors are installed on Malmbanan. In this paper, data from the detector at *Sunderbyn*, see Figure 1, has been analysed. The detection zone, covering a distance exceeding the wheel circumference, includes vertical force sensors mounted on the rail seats of eight consecutive sleepers [14]. At the time of the measurements, the Sunderbyn detector recorded mixed traffic conditions, including up to four loaded iron ore trains per day, freight traffic with a large variation in train speeds and axle loads, as well as passenger traffic with speeds up to 140 km/h. For each passing wheel, the detector measures the mean load F_{mean} and the peak load F_{peak}. From these data, the dynamic load $F_{\text{dyn}} = F_{\text{peak}} - F_{\text{mean}}$ is determined. Other data, such as the time of the measurement, traffic operator and train speed, are also recorded.

In Sweden, the winter 2017/2018 was particularly severe with low temperatures and high levels of snow precipitation. Overall, this resulted in a high number of alarms leading to a total of 1600 hours of train delays due to required rail inspections according to regulations.

For the different categories of traffic on Malmbanan, detector data measured over the time period from 1 October 2017–1 April 2018 (six months) have been collected and evaluated. As it was concluded that the maximum peak loads were generated by the 'freight' traffic category (*i.e.* including several different types of freight vehicles in empty and loaded conditions but excluding the fleet of iron ore trains), the effect of this particular type of traffic will be further analysed in this paper. More specifically, freight traffic with axle load 20 tonnes and train speed 100 km/h will be taken as a reference load scenario representing common conditions with a high number of severe impact loads measured in the Sunderbyn detector, cf. Figure 2.

Figure 1. Wheel impact load detector [14] at Sunderbyn. Photo by Matthias Asplund, Swedish Transport Administration.

For the 'freight' category trains, the numbers of occurrences of peak load and dynamic load magnitudes versus different levels of axle load are shown in Figure 2(a,b). The range of each axle load bin is 2.5 tonnes, while the range of each dynamic load bin is 5 kN. Note that each figure shows a top view of the histogram and that each number of occurrences is plotted in logarithmic scale to increase the resolution. The influence of the range of train speeds on peak load is shown in Figure 2(c). Here, the range of each train speed bin is 10 km/h. A substantial scatter in the data with large variations in axle load and train speed and several cases of extreme impact loads are observed. Based on all studied 'freight' category measurements on the rail referred to as the 'right rail' in the detector database, the alarm limit 350 kN was exceeded five times during the six winter months with a maximum peak load of 455 kN (measured for axle load 20 tonnes and train speed 90 km/h, cf. Figure 2). The maximum dynamic load was 360 kN, while 1 permille of the passing wheels generated dynamic loads exceeding 154 kN.

For all 'freight' category wheels with axle load in the bins ≥20 tonnes (and all train speeds) that were measured during the month of March in 2018 (a month with a particularly high number of extreme impact loads), a histogram of the dynamic loads is shown in Figure 2(d). A zoom of the same histogram for the most extreme dynamic loads is illustrated in Figure 2(e). For this month, 1 permille of the passing wheels generated dynamic loads exceeding 170 kN. Different continuous probability distributions for a positive random variable θ have been applied to fit the histogram. In general, it was found that the three-parameter Burr type XII distribution provided a better fit than the alternative two-parameter lognormal and Gamma distributions that were tried. The corresponding cumulative distributions are presented in Figure 2(f). Note that the cumulative data and the fitted cumulative Burr distribution are almost overlapping. The cumulative distribution function of the Burr type XII distribution is written as, see [15,16],

$$F(\theta|\alpha, c, k)) = 1 - \frac{1}{\left\{1 + \left(\frac{\theta}{\alpha}\right)^c\right\}^k}, \theta > 0, \alpha > 0, c > 0, k > 0 \quad (1)$$

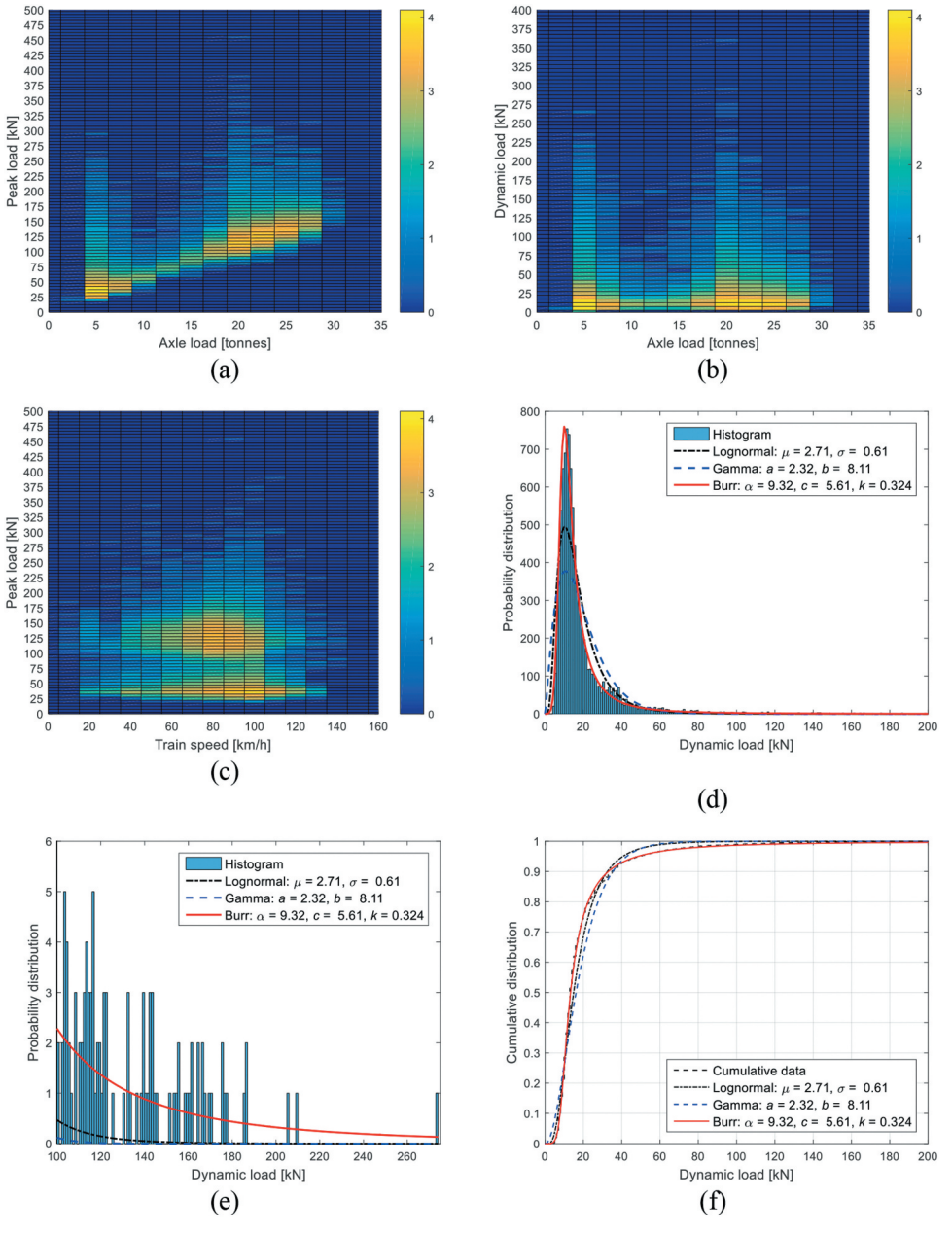

Figure 2. Data from right rail in the wheel impact load detector at Sunderbyn: 'freight' traffic with 126 770 measured wheels from 1 October 2017–1 April 2018. Numbers of occurrences (in logarithmic scale; for example, 4 corresponds to 10^4 wheels) of (a) peak load *vs*. axle load, (b) dynamic load *vs*. axle load, (c) peak load *vs*. train speed. (d) Histogram and probability distributions evaluated for 9 390 wheels (March 2018 – right rail) with axle load in bins ≥ 20 tonnes, (e) zoom of previous figure illustrating the most extreme measured loads, (f) corresponding cumulative distributions.

where c and k are shape parameters and α is the scale parameter. For an assessment of the matched tail distribution of extreme dynamic loads, note that the fitted Burr type XII distribution shown in Figure 2(e) predicts that 5 permille of the dynamic loads exceed 170

kN. Thus, the load distribution that will be applied in the following demonstration of calculation of probability of failure (see below) will be conservative in the sense that the probability of extreme dynamic loads is higher in the simulation than in this particular data set (March 2018 – right rail). On the other hand, the fitted lognormal and Gamma distributions predict that 170 kN is exceeded by only 0.03 permille and 0.00004 permille of the dynamic loads, respectively.

For comparison, the *iron ore traffic* (not shown here) is dominated by loaded trains with nominal axle load 30 tonnes at nominal speed 60 km/h and unloaded trains with axle load 5 tonnes at nominal speed 70 km/h. The maximum measured peak load was 314 kN. Most of the wheels on the iron ore trains induced low dynamic loads (about 90% of the wheel passages generated a dynamic load lower than 20 kN). Despite the high axle loads, and consequently high mean loads, no wheel triggered the alarm limit, indicating that the wheels on the iron ore fleet are generally in good condition.

3. Linear elastic fracture mechanics

A linear elastic fracture mechanics (LEFM) approach is employed to determine the stress intensity at a pre-existing rail foot crack subjected to combined bending and temperature loading [11,12]. The considered case is illustrated in Figure 3. It is assumed that the crack is loaded by uni-axial tensile stresses due to rail bending and temperature-induced thermal loads. A single crack is considered meaning that the influence of any nearby cracks is ignored. Note that the influence of residual stresses from manufacturing is neglected. For the current study of fracture setting out from a propagating fatigue crack, this simplification is deemed acceptable since the crack propagation under dynamic loading has to a large extent reduced (and redistributed) pre-existing residual stresses, cf [3,11].

Presuming Euler–Bernoulli beam theory to be valid, a time-variant rail bending moment M_y corresponds to a time-variant normal stress in the rail foot as

$$\sigma_{\mathrm{b}}(t) = M_y(t) \cdot h_{\mathrm{f}}/I_y \tag{2}$$

with the sign convention that a positive bending moment generates a tensile stress in the rail foot. Further, I_y is the cross-sectional moment of inertia and h_{f} is the distance defined in Figure 3. Thermal loading (assuming a continuously welded rail) is accounted for as an additional (uniform) normal stress

$$\sigma_{\mathrm{T}} = E\alpha\Delta T \tag{3}$$

where E = 210 [GPa] is the Young's modulus and α = 11.5 $\cdot 10^{-6}$ [°C^{-1}] is the thermal expansion coefficient. The rail temperature difference $\Delta T = T_0 - T$, where T_0 is the stress-free temperature and T is the current rail temperature. Thus, $\Delta T > 0$ corresponds to a tensile stress.

From the evaluated stresses, the mode I stress intensity factor at the pre-existing rail foot crack is derived as

$$K_{\mathrm{I}}(a_{\mathrm{f}}, b_{\mathrm{f}}, t) = f(a_{\mathrm{f}}, b_{\mathrm{f}}) \cdot \sigma(t)\sqrt{\pi a_{\mathrm{f}}} \tag{4}$$

Here a_f is the initial crack length as defined in Figure 3 and $\sigma(t)$ is the time-variant normal stress taken as the sum of $\sigma_b(t)$ according to Equation (2) for bending and σ_T according to Equation (3) for the thermal loading. Thus, $\sigma(t) = \sigma_b(t) + \sigma_T$. Further $f(a_f, b_f)$ is a geometry factor that for a rail foot crack can be approximated from the standard case of an edge crack in a plate subjected to uni-axial tension, [17], as

$$f(a_f, b_f) = \frac{\sqrt{\frac{2b_f}{\pi a_f}}}{\cos\left(\frac{\pi a_f}{2b_f}\right)} \cdot \left\{0.752 + 2.02\left(\frac{a_f}{b_f}\right) + 0.37\left(1 - \sin\left(\frac{\pi a_f}{2b_f}\right)\right)^3\right\} \tag{5}$$

For the purpose of the current study, this geometry factor is considered as a sufficient approximation for both bending and pure tension. To account for varying load magnitudes and interaction between bending and temperature loading, the assumption of LEFM (together with the fact that both the bending and temperature difference impose mode I loading) allows for scaling and summing of stress intensity factors [11].

The fracture criterion under LEFM conditions can be expressed as

$$\max_t\{K_I(t)\} \geq K_{Ic} \tag{6}$$

Here K_{Ic} is the fracture toughness of the rail material. For the current case of combined bending and thermal loading, the fracture criterion is formulated as

$$\max_t\{K_{Ib}(t) + K_{IT}\} \geq K_{Ic} \tag{7}$$

In this paper, for each wheel passage, the time-variant contribution to the stress intensity will be evaluated based on a simulation of dynamic vehicle–track interaction, see Section 4. Since the bulk rail temperature will remain constant during a wheel passage, the maximum stress intensity is obtained when the generated rail bending moment induced by the wheel passage is maximum.

When the fracture criterion (7) is fulfilled, the crack will be subjected to static fracture. In general, this need not result in complete fracture if there exists a stress gradient. However, for the current case a rail break will often occur since the bending stress

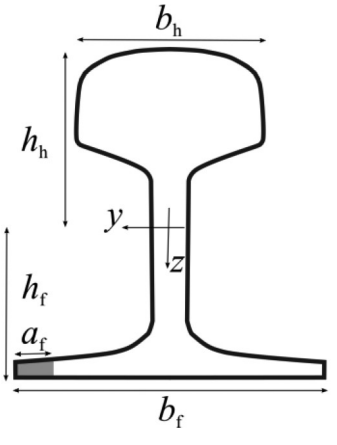

Figure 3. Studied geometry of rail foot crack. For a nominal 60E1 rail profile, $I_y = 30.55 \cdot 10^{-6}$ m^4 and $h_f = 0.081$ m.

gradient is rather shallow and the thermal stress often substantial. Note however that a single rail break usually does not cause a derailment [18]. It is, however, a safety issue, may result in secondary damage, and will cause traffic disruptions especially when the signalling system indicates rail break.

4. Dynamic vehicle–track interaction

A discrete wheel tread defect is a local deviation from the nominal wheel radius along a short section of the wheel circumference. This deviation introduces a radial irregularity that may generate an impact load in the wheel–rail contact. In this paper, the term *impact* refers to a situation with a transient vertical wheel–rail contact loading resulting in a maximum of the contact force that is high relative to the mean (quasi-static) wheel load but not necessarily leading to a momentary loss of contact, cf [6]. With each wheel revolution, the loading is a repeated event exciting vibration in a wide frequency range with most of the energy concentrated up to about 1 kHz. For the numerical prediction of high-magnitude loading and situations potentially leading to loss of contact, a non-linear wheel–rail contact model is required, implying that the simulation of dynamic vehicle–track interaction is carried out in the time domain.

In this paper, the vertical dynamic wheel–rail contact force and rail bending moment are solved using a time-domain model [19]. A sketch of the applied model is shown in Figure 4. Symmetric vehicle and track properties with reference to the centre of the track, and a symmetric excitation due to the same shape of a wheel tread irregularity on both wheels in the wheelset, are assumed. This means that only the wheels on one side of the wheelsets and one of the rails need to be included in the model.

For simulations of wheel–rail impact, it is generally sufficient that the vehicle model only includes one wheelset (the unsprung mass) since the primary suspension isolates the vehicle from the wheelset in the frequency range of interest. However, for an accurate prediction of the magnitude of the rail bending moment, the loading from several adjacent wheelsets needs to be accounted for. For the input data used in the present track model, it was found that the additional influence of adding more wheelsets in the model than the two in one bogie was negligible. A finite element model is required to capture the high-frequency dynamics and eigenmodes of the wheelset. However, in this paper, a simplified wheelset model is used, see Figure 4 and [20,21], which contains two degrees of freedom (dofs). The large mass M_w = 712.5 kg corresponds to the unsprung mass of half of a SJ57H freight wheelset. The values of the non-physical parameters, the small mass m_w (3 kg), the spring stiffness k_w (1650 kN/mm) and the damper c_w (5.4 kNs/m), have been tuned to better match the receptance at the wheel–rail contact with the corresponding receptance calculated using a detailed FE model of the wheelset, see [22]. Most resonances and antiresonances of the wheelset cannot be captured with the simplified model, but the average trend of the wheelset receptance above the tuned resonance is similar between the simplified and the detailed models. It has been verified (not shown here) that the selected simple wheelset model leads to similar rail bending moments as a more advanced and more computationally demanding Craig–Bampton model (accounting for several wheelset modes). As an example, it was found that for the present application with flat depth 2 mm, the Craig–Bampton model resulted in 8%

lower impact load and 3% higher maximum rail bending moment than the simple wheelset model, while the simulation time increased by about a factor of 4.

The track model includes one discretely supported 60E1 rail modelled by Rayleigh–Timoshenko beam theory accounting for shear deformation and rotatory inertia. The vertical and rotational stiffnesses and damping of each rail pad are modelled as two sets of spring and damper coupled in parallel (Kelvin model), while each half sleeper is modelled as a discrete rigid mass. The combined stiffness and damping of the ballast and subgrade below each sleeper are represented by another Kelvin model. Input data to the track model, see the Appendix, is taken from [21] where the simulation model was validated versus field measurements of wheel–rail contact force using an instrumented wheelset. To reduce the time for simulation of dynamic vehicle–track interaction, the track model is taken as linear and a complex-valued modal approach with a truncated mode set is applied. In order to obtain a discrete spectrum of eigenvalues, a finite length of the track is required. This means that wave reflections from the track model boundaries will occur and structure-borne vibrational energy cannot be transmitted away from the structure. In the present study, it was found that a track model containing 70 sleeper bays and clamped ends at both rail boundaries is sufficient for prediction accuracy if the impact loads and rail bending moment are evaluated at the centre of the track model. In a previous study [23], for a known combination of static and dynamic wheel loads measured in a wheel impact load detector (not the same detector as in Sunderbyn) and using a similar simulation model but with other calibrated levels of track stiffness, good agreement between calculated and measured rail bending moments was observed.

As discussed above, discrete wheel tread irregularities can, for example, be caused by rolling contact fatigue or be a consequence of wheel sliding without rolling (wheel flats).

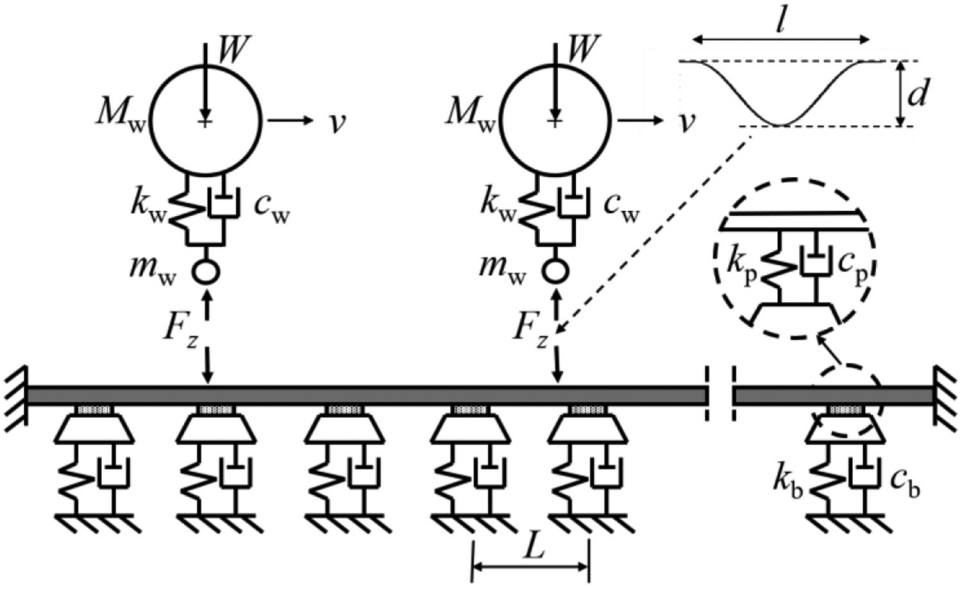

Figure 4. Model for simulation of dynamic vehicle–track interaction accounting for the influence of a tread irregularity with length *l* and depth *d* on the leading wheel.

The magnitude of the impact load is influenced by the three-dimensional shape of the irregularity. In this paper, it is assumed that all impact loads are generated by an irregularity that can be described by a simple mathematical expression in one dimension. A new wheel flat with sharp edges can be described as a chord of the wheel circumference, where the length l_0 and depth d are approximately related by

$$l_0 \approx \sqrt{8R_w d} \tag{8}$$

Here, R_w = 0.45 m is the wheel radius and it is assumed that $d \ll R_w$. However, the corners (edges) of a new wheel flat are soon rounded due to wear and plastic deformation caused by repeated wheel–rail impacts. According to [24], the radial wheel profile deviation x_{rf} for a flat with rounded edges and length l can be approximated as

$$x_{rf} = \frac{d}{2}\left\{1 + \cos\frac{2\pi z}{l}\right\}, -\frac{l}{2} \le z \le \frac{l}{2} \tag{9}$$

where z is an arc coordinate along the flat. Here it is assumed that the depths of the new and rounded flats are the same but $l > l_0$, cf [25]. Wheel flats introduce a vertical relative displacement input to the wheel–rail contact. For a new flat, the wheel pivots around the two corners, and the wheel trajectory differs from the shape of the flat due to the curvature of the wheel. Assuming the rounded edges of the flat can be described by a quadratic function with smooth transitions, and the lateral contact position on the wheel remains constant at where the tread irregularity has its maximum, the wheel centre vertical trajectory x_w can be written as, [20],

$$x_w \approx \begin{cases} 4d\{(2z + l)/2l\}^2, & -l/2 \le z \le 0 \\ 4d\{(l - 2z)/2l\}^2, & 0 \le z \le l/2 \end{cases} \tag{10}$$

This formula can be used for both new and rounded wheel flats [20], and it represents the prescribed relative wheel–rail vertical displacement excitation used as input in the simulation of dynamic vehicle–track interaction [6].

The influence of wheel–rail contact model on calculated impact loads due to new and rounded wheel flats was investigated in [26]. A three-dimensional non-Hertzian contact model based on Kalker's variational method [27], a two-dimensional non-Hertzian contact model consisting of a Winkler bed of independent springs [28], and a single non-linear Hertzian contact spring (point contact model) [29] were compared. The relative displacement excitation used as input to the Hertzian model was the pre-calculated wheel centre trajectory in Eq. (10). For rounded flats, both the two-dimensional model and the Hertzian spring model were found to generate results in good agreement with the three-dimensional model. Thus, in this paper, the contact model used in the simulation is a single Hertzian spring (point contact model) [26]. The force–displacement characteristic of this spring is expressed as

$$F_{w/r} = C_H\langle\delta\rangle^{3/2} \tag{11}$$

where δ is the approach distance of two distant points on wheel and rail, while the factor C_H is a function of material parameters and the principal relative radii of curvature. The Macaulay brackets are defined as $\langle\bullet\rangle = 0.5(\bullet + |\bullet|)$. Thus, $F_{w/r} = 0$ if $\delta < 0$ (loss of contact).

In a parameter study, the simulation model described in this section has been applied to calculate the influence of wheel flat depth d on the dynamic wheel–rail impact load F_{dyn}, see Figure 5. As discussed in Section 2, train speed and axle load were set to 100 km/h and 20 tonnes, respectively, as this can be regarded as a representative setting with reference to the conditions at the Sunderbyn detector. For each depth d, Eqs. (8) and (10) with $l = 1.50 \cdot l_0$ were used to formulate the excitation input. For each depth d, the simulation was repeated for eight impact positions, indicated by the circles in Figure 5, equidistantly distributed over one sleeper bay. It is observed that the influence of impact position within a sleeper bay on the evaluated impact load is significant and increases with increasing flat depth, cf [26]. An example of calculated wheel–rail contact force and rail bending moment at the centre of a sleeper bay is shown in Figure 6. Note that a wheel–rail impact at the centre of a sleeper bay is a worst-case scenario in terms of the maximum rail bending moment and the position of the pre-existing crack.

Using a regression analysis for all the calculated dynamic loads in Figure 5, a meta-model based on a polynomial of order $N = 9$ has been derived as

$$F_{\mathrm{dyn}} = \sum_{n=1}^{N} \alpha_n d^n \tag{12}$$

The meta-model, with the constants α_n calibrated for $0 \leq d \leq 7$ mm given in the Appendix, is shown as the solid line in Figure 5. For the given combination of train speed, axle load and input data to the vehicle and track models used in this paper, this meta-model is implemented as a mapping between the dynamic load measured in the Sunderbyn detector and the flat depth used in the simulation model. By solving for d in Eq. (12) for each given F_{dyn}, the probabilistic distribution of dynamic loads measured in the detector is transformed to a corresponding stochastic distribution of wheel tread irregularities specified by d (and l via Eq. (8)). In this way, a similar representative distribution of dynamic loads is achieved for the simulation model as was measured in the detector, irrespective of the type of discrete tread defect that generated the measured impact.

The same distribution of wheel tread irregularities could be applied in combination with another set of input data for the vehicle and track models. For example, it can be expected that sleeper support conditions (ballast/subgrade stiffness, presence of hanging sleepers, etc.) vary along the track, having a substantial influence on the magnitudes of rail bending moments and the risk of rail breaks. Since different vehicle and track properties influence the dynamics of the vehicle–track system, the same distribution of wheel tread irregularities would result in another distribution of dynamic loads than the one measured in the Sunderbyn detector. Such studies could also be employed to, for example, investigate the relative influence of a different axle load, train speed or track stiffness. Note that since the input data to the track model applied in this paper has not been calibrated versus the absolute conditions at the Sunderbyn detector, all such studies would be in relative terms. For example, what is the increased risk for a rail break if the sleeper support stiffness is halved compared to the support stiffness used in the track model for the Sunderbyn detector.

As pointed out above, the true three-dimensional shapes of wheel tread irregularities passing over the detector at Sunderbyn can be expected to be more complex than the

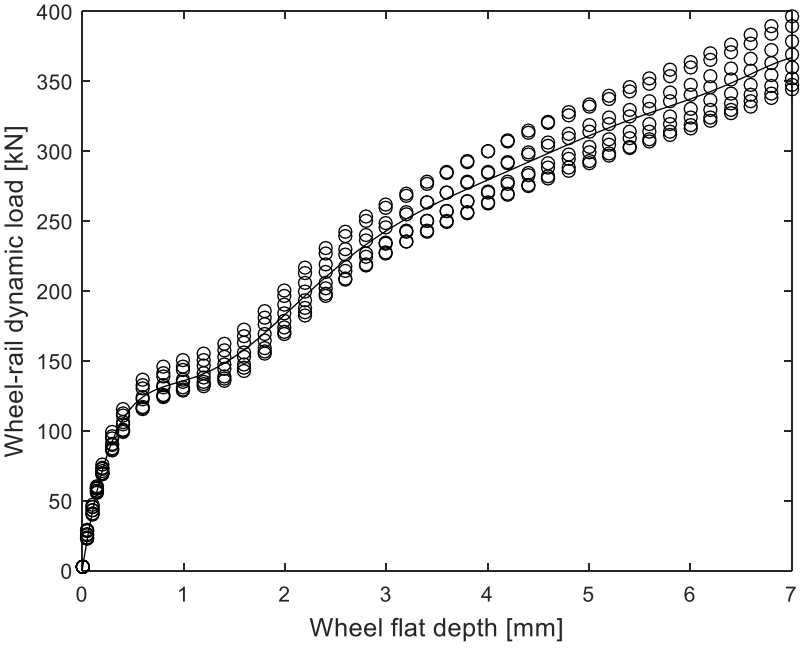

Figure 5. Calculated influence of wheel flat depth on wheel–rail dynamic load. Rounded flat with $l = 1.50l_0$. Hertzian contact model with pre-calculated wheel centre trajectory as input. For each flat depth, 8 simulations were carried out to cover the range of impact positions relative to the discrete supports. Solid line is a meta-model based on a 9th-order polynomial. Axle load 20 tonnes, train speed 100 km/h and vehicle/track input data according to Section 4 and the Appendix.

geometry represented by Eq. (9). However, as long as the measurements in the detector can be regarded as accurate, using the meta-model in Eq. (12) in combination with the measured distribution of dynamic loads and applying a stochastic spread in impact positions will lead to a representative stochastic representation of the dynamic loading that is affecting the pre-existing crack.

5. Probability of rail break

In this paper, the probability of the rare event of an instant rail break corresponds to the probability of an occurring load case leading to that the maximum stress intensity at the pre-existing rail foot crack exceeds the fracture toughness. Based on Eq. (7), the performance function g is defined as

$$g(\theta_1, \theta_2, \ \ldots \ , \ \theta_M) = K_{\mathrm{Ic}} - K_{\mathrm{IT}} - \max_t\{K_{\mathrm{Ib}}\} \tag{13}$$

where θ_i, $i = 1, 2, \ldots M$, are stochastic variables with prescribed probability distribution functions $\varphi(\theta_i)$. Here, two (M= 2) stochastic variables influencing the maximum stress intensity will be considered. These are the impact position θ_1 relative to the position of the crack and the magnitude θ_2 of the dynamic load.

If $g < 0$ for a given setting of the stochastic variables, the rail is considered as being failed (instant rail break). Considering the stochastic distributions of variables θ_i, the

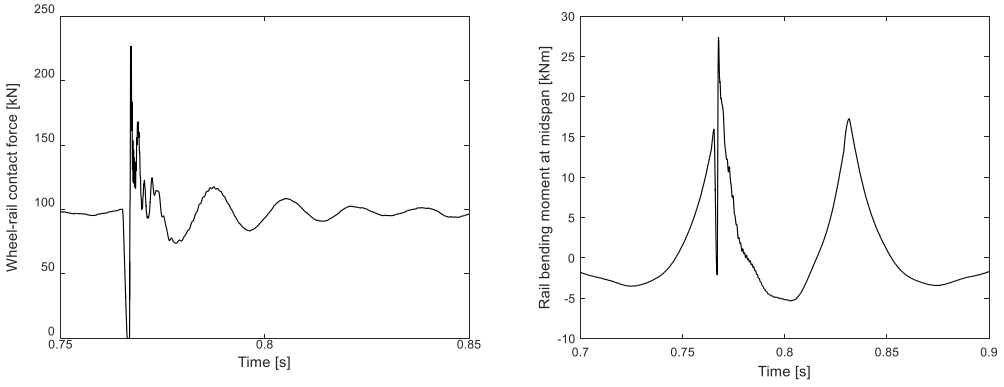

Figure 6. Calculated time histories of wheel–rail contact force and rail bending moment at sleeper bay midspan. Axle load 20 tonnes, train speed 100 km/h, wheel flat with $l = 90$ mm and $d = 1$ mm making impact at sleeper bay midspan. Vehicle/track input data according to Section 4 and the Appendix.

probability of failure P_f is determined as the probability of $g < 0$. The hyper-surface defined by $g = 0$ is the limit state.

Assuming there is only one significant tread irregularity around the wheel circumference, the position θ_1 has a uniform probability distribution $\varphi_U(\theta_1)$ along with a distance corresponding to the wheel circumference. Here, the interval of θ_1 is taken as $-\pi R_w < \theta_1 < \pi R_w$, where $\theta_1 = 0$ corresponds to the case where the centre of the wheel tread irregularity is aligned with the position of the pre-existing crack. Thus, all impact positions along with a distance corresponding to the wheel circumference are equally probable. For a quasi-static excitation of a track without hanging sleepers, the maximum bending moment along the rail is generated at the centre of a sleeper bay. The origin of θ_1 and the position of the initial crack is assumed to be at this position, and the rail bending moment is calculated at $\theta_1 = 0$ independent of impact position. For a rail foot crack in a uniformly supported track without hanging sleepers, this corresponds to a worst-case scenario in terms of crack position. The magnitude θ_2 of the dynamic load is determined by the Burr type XII distribution $\varphi_B(\theta_2)$presented in Section 2, which is transformed to a corresponding depth of the prescribed wheel tread irregularity using Eq. (12). Note that $\Phi_B(\theta_2{=}1)$ has been set to 360 kN as this was the maximum dynamic load measured in the detector. For each combination of stochastic variables, the cumulative distributions $\Phi_U(\theta_1)$ and $\Phi_B(\theta_2)$ $(0 \leq \Phi_i \leq 1, i = U, B)$ are applied to sample the input data used in the simulations of dynamic vehicle–track interaction and calculations of rail bending moment.

Standard Monte Carlo (MC) simulation is a robust approach for the calculation of probability of failure. However, the computational cost can be very high if a small probability, corresponding to the tail distribution of the response quantity, needs to be determined. In this paper, the subset simulation (SS) algorithm presented in [9] will be used to calculate the probability of a rail break. It is an advanced Monte Carlo method that employs a multi-level Markov chain Monte Carlo (MCMC) sampling technique to

adaptively generate samples from the (rare event) fail region(s) in the stochastic parameter space. The strategy of SS is to break down the rare event problem into a sequence of more frequent-nested events and determine the failure probability as a product of conditional probabilities, each of them being estimated by a MCMC simulation. In Section 7, the accuracy of the SS-algorithm will be assessed by comparison with MC simulations. Based on a convergence study (not shown here), each standard MC simulation will be based on $3{\cdot}10^6$ samples of the performance function. For each simulation with the SS-algorithm, six levels will be used, each level with $1{\cdot}10^4$ samples and probability 0.1, cf [9]. For both methods, the probability of failure will be taken as the mean value of 20 simulations.

It is evident that a prediction of the probability of an instant rail break could involve further stochastic variables besides the variations in dynamic load and impact position. For example, the thermal loading of the rail varies around the year. Fracture toughness K_{Ic} and the position and initial length of any pre-existing rail crack are other parameters with a stochastic spread. According to EN13674-1:2011 [30], the minimum single value for K_{Ic} in the R350LHT rails used on Malmbanan is 26 MPa$\sqrt{\mathrm{m}}$ (nominal value 40 MPa$\sqrt{\mathrm{m}}$), while the acceptable crack length in the heat-treated rails is 3 mm. In this paper, these parameters will be taken as deterministic, but their influences will be investigated in a parameter study in Section 7. Note that the influence of the spread in train speeds has already been considered by fitting the probability distribution of dynamic loads to the field data presented in Figure 2.

6. Meta-model of performance function

The computational cost for predicting the probability of a rare event instant rail break due to a wheel–rail impact load can be reduced by using a meta-model $\hat{g}(\theta_1, \theta_2)$ of the performance function. In this paper, the meta-model is generated by application of a thin plate spline [31], see the function *tpaps.m* in Matlab [32]. It is a type of meshfree approximation method using radial basis functions that allows for scattered data [33]. The thin plate spline is a type of poly-harmonic spline in two dimensions.

Based on the cumulative distributions $\Phi_{\mathrm{U}}(\theta_1)$ and $\Phi_{\mathrm{B}}(\theta_2)$, the meta-model is generated by a grid sampling approach. An iterative process is applied, where the studied samples are concentrated to the fail region (i.e. where $g < 0$) and around the limit state to reduce the error in the domain of the meta-model that is significant for the evaluation of the probability of failure. Before the iterative process is started, an initial screening of the performance function over the stochastic space is performed using a 9×9 grid of equidistant samples between 0 and 1 for each variable. If > 0 for all of these 81 samples, simulations are repeated using a smaller grid with new samples near $\Phi_{\mathrm{U}}(\theta_1) = 0.5$, $\Phi_{\mathrm{B}}(\theta_2) = 1$ as this can be expected to be the region where g has its minimum. Note that the worst load case is generally when the wheel impact occurs exactly above the crack. Since it is the far end of the irregularity that makes impact with the rail, this means that the position of the circumferential centre of the wheel tread irregularity is at a position shortly ahead of the crack, typically in the range $0.45 < \Phi_{\mathrm{U}}(\theta_1) < 0.5$.

In each iteration, the minimum and maximum values of each variable Φ_i leading to $g < 0$ are determined to specify the boundaries of a new grid for which the performance

function is evaluated. In the subsequent iteration, the distance between evaluated samples of Φ_i is halved compared to the previous grid. In this way, the domain where $g< 0$ is evaluated in increasing detail. Using the SS-algorithm, the normalized error e in calculated probability between two subsequent iterations is calculated. If $e > e_{\text{lim}}$, a new iteration is performed (in this paper, $e_{\text{lim}} = 0.10$). The root mean square error of $\hat{g}$ is also monitored to ensure that $\hat{g}$ has a good fit with all samples of g. Note that the accuracy of the meta-model in the safe region, i.e. where $g > 0$, is of lesser importance.

The iterative process to reduce the error e is illustrated in Figure 7, where each sample where g has been evaluated is marked with an ×. An example of a meta-model of the performance function is presented in Figure 8. It is observed that the meta-model is positive and flat in most of the stochastic space. This is because the present Burr distribution leads to low dynamic loads, not significantly affecting the dynamic variation in stress intensity, up to about $\Phi_B(\theta_2) = 0.95$. For higher values of $\Phi_B(\theta_2)$, in the region around $\Phi_U(\theta_1) = 0.47$, there is a local minimum in the meta-model where $\hat{g} < 0$ because this corresponds to the most extreme dynamic load making impact directly above the pre-existing crack. The other two local minima in the meta-model at $\Phi_U(\theta_1) = 0.06$ and $\Phi_U(\theta_1) = 0.25$ ($\Phi_B(\theta_2) = 1.0$) are because the most extreme depths of the wheel irregularity generate a transient response where the wheel is bouncing on the rail and thus creating several local load maxima in contact force. If such a local maximum coincides with the crack position, the rail bending moment has a local maximum. The spurious (false) overshoots of the generated meta-model observed in the region before the performance function drops below zero has no significant influence on the predicted probability of failure.

For the application in this paper, it has been observed that the thin plate spline is unable to generate a good fit if the number of samples exceeds about 600. This typically corresponds to 5 or 6 iterations with the present grid sampling approach. For cases with a single fail region, this has been found to be sufficient leading to low errors e. However, cases with a combination of a long crack and low fracture toughness may lead to two (or more) isolated fail regions. In these cases, the number of iterations necessary to generate an accurate meta-model may result in that the number of samples exceeds 600 with the consequence that the root mean square error of $\hat{g}$ becomes high. The reason for the poorer fit could be a close to singular interpolation matrix when determining the coefficients of the thin plate spline, see [33]. This means that the assessment of cases with high-evaluated probabilities of rail break (where multiple domains of the performance function are below the limit state) are less accurate. The higher calculated values of risk presented in Section 7 should therefore be considered as indicative. It can be argued that such situations should be avoided by proper monitoring of crack lengths and selecting a high-quality rail grade with small variations in fracture toughness.

Note that a meta-model is an approximate model that generally cannot capture the exact features of the system. Several alternative types of meta-models are available [10]. It was found (not shown here) that a two-variable polynomial model of high order and including cross-terms was not as accurate as the thin plate spline used in this paper. However, according to Figure 7, the thin plate spline seems to be unable to perfectly mimic the position of the limit state. This is observed by noting that in each iteration, according to the applied sampling approach, new samples are added to as closely as possible circumvent the region where $g < 0$. However, in Figure 7(d), the limit state

evaluated by $\hat{g} = 0$ after iteration 5 remains at approximately the same position as after iteration 4 even if the illustrated positions of the new samples of are indicating that the true limit state given by $g = 0$ should be towards lower values of Φ_B (i.e. $\hat{g} = 0$ is outside the region where the new samples have been added). Since this results in a larger fail region modelled by the meta-model, the predicted probability of rail break can be expected to be conservative. In future work, other types of meta-models could be evaluated to aim for higher accuracy around the limit state.

7. Numerical examples

To demonstrate the methodology presented in this paper, the probability of a rail break P_f is predicted for different combinations of initial crack length, fracture toughness and rail temperature difference. Note that the calculated probability is evaluated for the given statistical distribution of dynamic loads that was generated by the 'freight' category of trains on Malmbanan in March 2018, cf. Figure 2(d-Figure 2(f). This was a particularly severe month in terms of the number and magnitudes of extreme loads. To limit the maximum applied load in line with the maximum load measured during the winter 2017/2018, it is assumed that $\Phi_B(1)$= 360 kN. As discussed in Section 2, the applied loading of the crack is conservative in the sense that the tail of the fitted Burr type XII distribution leads to a higher number of extreme dynamic loads compared to what was measured in the detector. Further, it is assumed that the pre-existing rail foot crack is positioned in the centre of a sleeper bay. The combination of a high number of extreme dynamic loads and the assumed position for the crack forms a worst-case scenario.

On the other hand, the calculated probability is also based on the assumed input data for the given vehicle–track model. In this study, the track model is assumed to have uniform sleeper support conditions with a relatively high stiffness as this should be required for a well-maintained wheel impact load detector. A situation with worse support conditions in terms of lower ballast/subgrade stiffness or even the presence of occasional hanging sleepers would increase the maximum rail bending moment and increase the risk of a rail break. Further, the vehicle model represents a 'freight' bogie with axle load 20 tonnes and train speed 100 km/h as this was concluded to be a representative scenario for the detector at Sunderbyn, see Section 2. By using Eq. (12), which has been derived for this particular scenario of axle load, train speed and vehicle/track input data, the distribution of dynamic loads measured in the detector is transformed to a corresponding distribution of wheel tread irregularities (wheel flats described by length l and depth d).

The calculated stress intensity at the crack also considers the influence of thermal load because of a rail temperature difference ΔT. For each combination of initial crack length, fracture toughness and rail temperature difference, P_f is calculated by the subset simulation algorithm with the settings listed in Section 5 and using a meta-model $\hat{g}$ of the performance function as described in Section 6. Considering the stochastic distributions of variables θ_i, each value of P_f presented in Figures 8–10 is corresponding to the probability of $\hat{g}< 0$. It is the mean value calculated from 20 simulations of the loading. For the given vehicle–track model and the applied stochastic distributions of impact

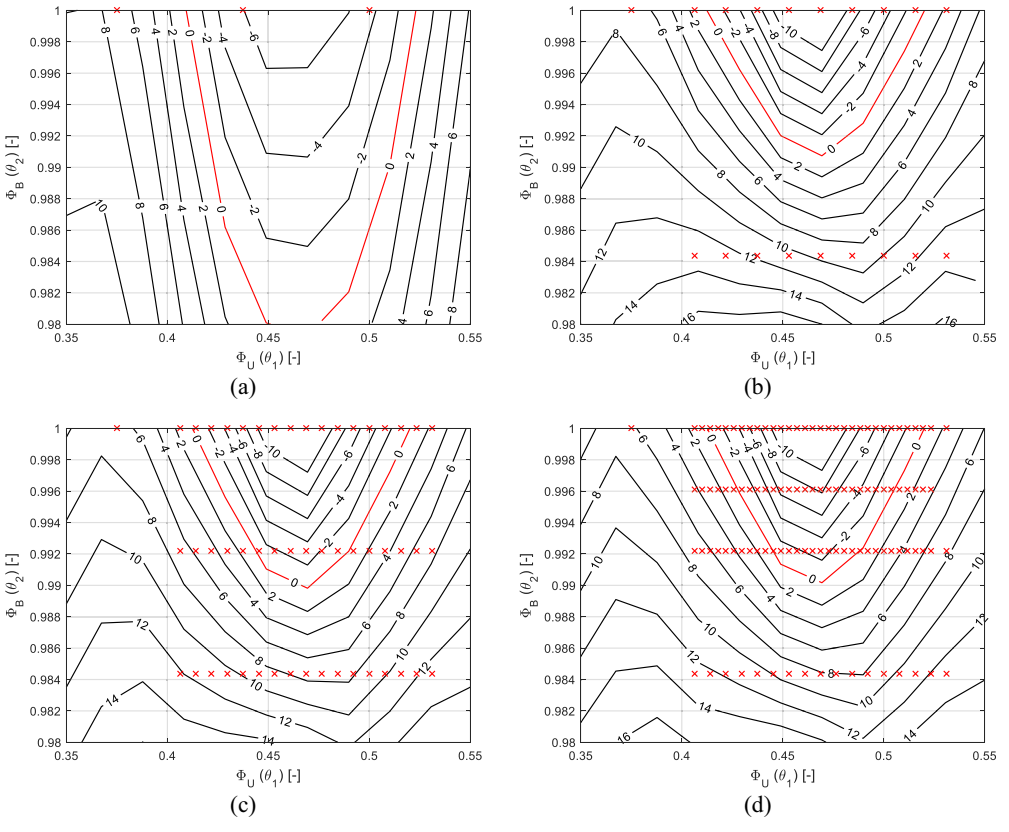

Figure 7. Demonstration of iterative process to improve meta-model and reduce error e of calculated probability of rail break P_f. The limit state $\widehat{g} = 0$ is marked with a red line, while samples where g has been evaluated are marked with ×. (a) Iteration 1: P_f = 1.7e-3, (b) iteration 3: P_f = 4.5e-4, e= 0.98, (c) iteration 4: P_f = 2.7e-4, e= 0.65, (d) iteration 5: P_f = 1.7e-4, e= 0.57. After seven iterations: P_f = 2.1e-4, e= 0.07. Initial rail foot crack length a_f = 10 mm, K_{Ic} = 40 $\mathbf{MPa}\sqrt{\mathbf{m}}$, ΔT= 30°C.

position and magnitude of dynamic load, the results should be interpreted in the sense that on the average *one wheel of 1/P_f wheel passages* generate a stress intensity at the pre-existing rail foot crack that could induce a rail break.

Based on the conditions and scenario described above and for a rail with uniform fracture toughness K_{Ic} = 40 MPa, the influences of initial crack length a_f and rail temperature difference ΔT on P_f are illustrated in Figure 9. For example, for the extreme case of a_f = 10 mm and ΔT= 40°C, $P_f = 4.2 \cdot 10^{-4}$. This corresponds to that one wheel in only 2400 wheel passages would generate a stress intensity at the pre-existing rail foot crack that could induce a rail break. For ΔT= 40°C, the risk has been calculated using both the SS-algorithm and standard MC simulation. Good agreement is observed between the two methods. However, with the settings listed in Section 5, the SS-algorithm is in the order of 40 times faster than the MC simulation. As expected, P_f increases with increasing length of the pre-existing crack. In this case, no risk of rail break was predicted for a_f < 4.75 mm. A kink in the curve is observed between crack lengths 9 and 10 mm. This is because the local minimum at $\Phi_U(\theta_1) = 0.25$, $\Phi_B(\theta_2) = 1.0$, cf. Figure 8, has dropped below the limit state introducing a second fail region. The agreement between the SS and MC simulations is acceptable also when there are two isolated fail

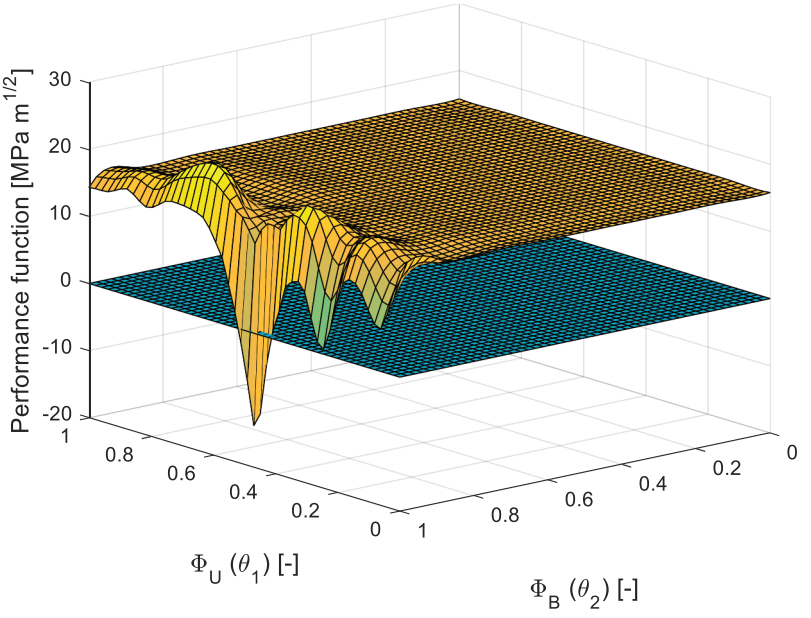

Figure 8. Example of meta-model $\widehat{g}$ of performance function. Initial rail foot crack length a_f = 10 mm, K_{Ic} = 40 MPa$\sqrt{m}$, ΔT= 30°C.

regions. Further, a significant influence of ΔT on P_f is observed. For example, for $\Delta T \leq$ 20°C, $P_f = 0$ if $a_f \leq 6.75$ mm.

For a_f = 5 mm, the influences of ΔT and K_{Ic} on P_f are illustrated in Figure 10. For example, for K_{Ic} = 40 MPa$\sqrt{m}$ and $\Delta T \leq$ 35°C, $P_f = 0$. However, as expected, with decreasing K_{Ic} there is a significantly increasing risk of rail break. Finally, for ΔT= 40°C, the influences of K_{Ic} and a_f on P_f are studied in Figure 11. For a_f = 3 mm, there is no risk for rail break unless $K_{Ic} <$ 32 MPa$\sqrt{m}$.

8. Concluding remarks

A methodology for predicting the probability of an instant rail break initiated at a pre-existing rail foot crack by a prescribed distribution of dynamic wheel loads (including cases with extreme wheel–rail impacts) has been presented. For a faster numerical assessment of the probability of failure, a thin plate spline regression was implemented to develop a meta-model of the performance function quantifying the stress intensity at the crack. The methodology was demonstrated by assuming a pre-existing rail foot crack in the centre of a sleeper bay and investigating the influences of initial crack length, fracture toughness and rail temperature difference on the risk for a rail break.

It was concluded that the thin plate spline was able to provide a good approximation of the performance function in the fail region. However, in future work, alternative meta-modelling techniques could be explored to aim for a refinement of the model around the limit state to further improve the accuracy of the predicted probability of failure. In addition, the alternative meta-model could account for more stochastic variables than the

two (impact load and impact position) studied in this paper, such as sleeper support stiffness, fracture toughness, initial crack length, and crack position within the sleeper bay. The probabilities of failure predicted by the subset simulation algorithm were found to be in good agreement with the corresponding predictions by standard Monte Carlo simulation at a significantly lower computational cost (factor in the order of 40).

For a given setting of vehicle and track input data, a procedure was introduced to map the probabilistic distribution of dynamic loads measured in the detector to a corresponding stochastic distribution of wheel tread irregularities used in the simulation model. In this way, a similar variation in dynamic loads was achieved for the simulation model as was measured in the detector. In a subsequent analysis, the same representative distribution of wheel tread irregularities could be applied with other input data for the vehicle and track models to study the relative influence of, for example, a different axle load, train speed or variations in track stiffness. The distribution of resulting dynamic loads and rail bending moments will be different compared to the baseline case as influenced by the change in input data. Although the calculated influence of input data is then only provided in relative terms since the absolute conditions in the detector are unknown, this can be an option to investigate other scenarios such as situations with a lower ballast/subgrade stiffness or the presence of hanging (unsupported) sleepers since this can be expected to increase the risk for rail breaks.

Note that extending this work to predict the probability of a rail break induced at a pre-existing crack in the rail head is possible presuming the head crack has deviated into transverse growth and is propagated by rail bending, see [12]. In that case, the load scenario leading to the maximum stress intensity at the crack is when one of the two wheels in a bogie is generating an impact on the rail at the same time as the crack is centred between these two wheels inducing an uplift of the rail.

Acknowledgements

The current work is part of the activities within the Centre of Excellence CHARMEC (CHAlmers Railway MEChanics, www.chalmers.se/charmec). Parts of the study have been funded within the European Union's Horizon 2020 research and innovation programme in the Shift2Rail project In2Track2 under grant agreement No. 826255. Input data has been supplied by Dr Matthias Asplund, Trafikverket (the Swedish Transport Administration).

Disclosure statement

No potential conflict of interest was reported by the authors.

References

[1] Nielsen JCO, Johansson A. Out-round wheels – a literature survey. Proceedings of the Institution of Mechanical Engineers, Journal of Rail and Rapid Transit. 2000;214:79–91.
[2] Nielsen JCO, Lundén R, Johansson A, et al. Train–track interaction and mechanisms of irregular wear on wheel and rail surfaces. Veh Syst Dyn. 2003;40(1–3):3–54.
[3] Ekberg A, Kabo E. Fatigue of railway wheels and rails under rolling contact and thermal loading – an overview. Wear. 2005;258:1288–1300.
[4] UIC: Prevention and mitigation of derailment (PMD), IRS 70729, 2019.

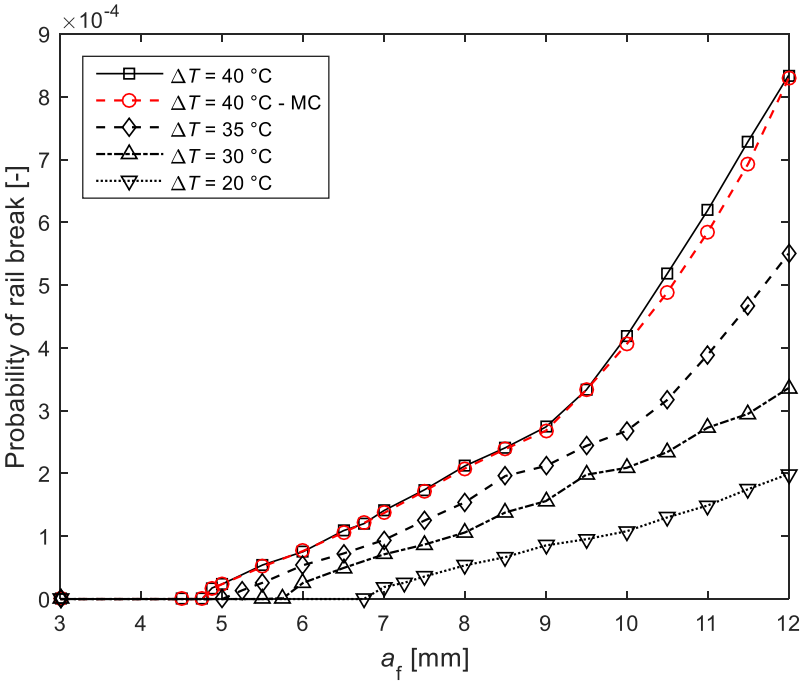

Figure 9. Influence of rail temperature difference and rail foot crack length on probability of rail break (mean value based on 20 simulations): K_{Ic} = 40 MPa$\sqrt{m}$. Axle load 20 tonnes, train speed 100 km/h, prescribed statistical distribution of dynamic loads as generated by the 'freight' category of trains on Malmbanan in March 2018, and vehicle/track input data according to Section 4 and the Appendix.

[5] D-RAIL: D1.1 – Summary report and database of derailments incidents, 2012, 71 + 3 pp, (http://d-rail-project.eu)
[6] Nielsen JCO, Pieringer A, Thompson DJ, et al. Wheel–rail impact loads, noise and vibration: A review of excitation mechanisms, prediction methods and mitigation measures. In: Degrande G. et al. (Editors). Noise and Vibration Mitigation for Rail Transportation Systems (Proceedings of the 13th International Workshop on Railway Noise; 2019; Ghent, Belgium), Notes on Numerical Fluid Mechanics and Multidisciplinary Design. Heidelberg: Springer; 2021.
[7] Rahrovani S, Lilja J, Abrahamsson TJS, et al. On the accuracy and efficiency of reliability methods applied in railway sleeper design. Department of Applied Mechanics, Chalmers University of Technology, Gothenburg, Sweden, 2016, 12 pp.
[8] Montgomery DC. Design and analysis of experiments. New York: Wiley; 1984.
[9] Au S-K, Beck JL. Estimation of small failure probabilities in high dimensions by subset simulation. Probab Eng Mech. 2001;16:263–277.
[10] Wang GG, Shan S. Review of metamodeling techniques in support of engineering design optimization. Transactions of the ASME. J Mech Des. 2007;129:370–380.
[11] Sandström J, Ekberg A. Predicting crack growth and risks of rail breaks due to wheel flat impacts in heavy haul operations. Proceedings of the Institution of Mechanical Engineers, J Rail Rapid Transit. 2009;223:153–161.
[12] Ekberg A, Kabo E, Nielsen JCO. Allowable wheel loads, crack sizes and inspection intervals to prevent rail breaks. Proceedings of the 11th International Heavy Haul Conference; 2015; Perth, Australia. p. 9.

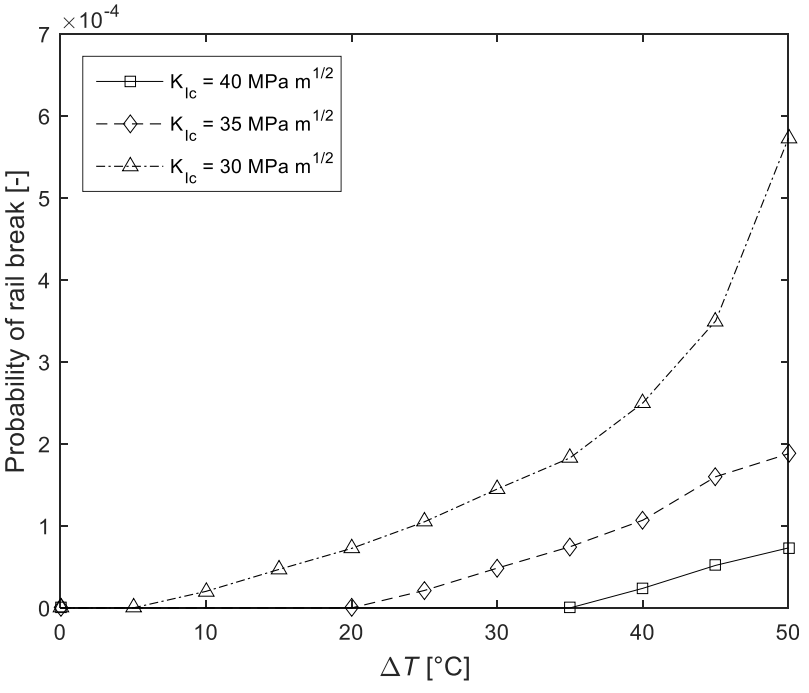

Figure 10. Influence of fracture toughness and rail temperature difference on probability of rail break (mean value based on 20 simulations): a_f = 5 mm. Other input data: see caption to Fig. 9.

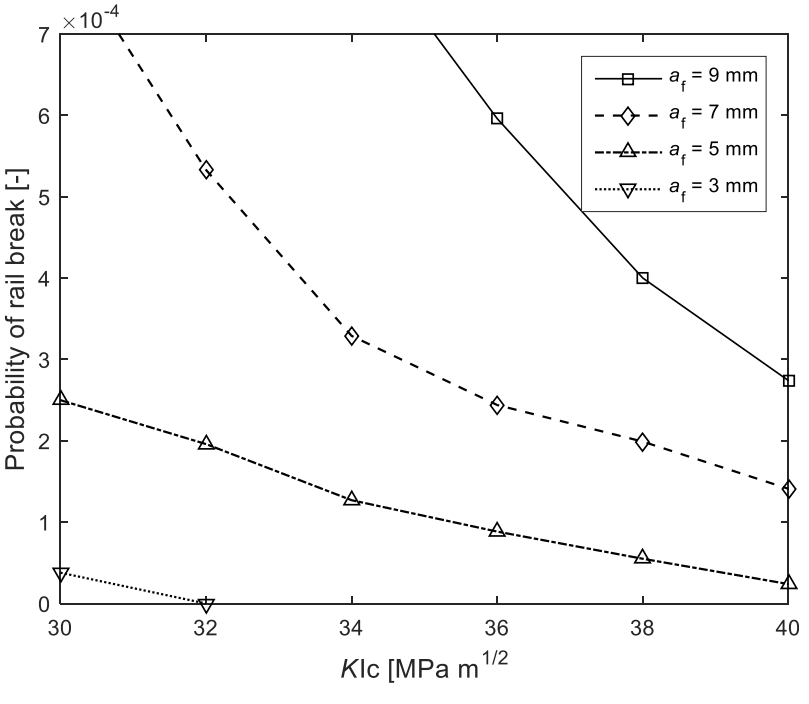

Figure 11. Influence of rail foot crack length and fracture toughness on probability of rail break (mean value based on 20 simulations): ΔT = 40°C. Other input data: see caption to Fig. 9.

[13] Nielsen JCO, Ringsberg JW, Baeza L. Influence of railway wheel flat impact on crack growth in rails. Proceedings of the 8th International Heavy Haul Conference; 2005; Rio de Janeiro, Brazil. p.8
[14] Schenck Process. MULTIRAIL WheelScan. [cited 2020 Dec 04]. Available from: https://www.schenckprocess.com/products/wheel-diagnosis-wheelscan
[15] Burr IW. Cumulative frequency functions. Ann Math Stat. 1942;13(2):215–232.
[16] Tadikamalla PR. A look at the Burr and related distributions. Int Stat Rev. 1980;48(3):337–344.
[17] Tada H, Paris PC, Irwin GR. The stress analysis of cracks handbook. New York: ASME Press; 2000.
[18] Magel E, Mutton P, Ekberg A, et al. Rolling contact fatigue, wear and broken rail derailments. Wear. 2016;366:249–257.
[19] Nielsen JCO, Igeland A. Vertical dynamic interaction between train and track – influence of wheel and track imperfections. J Sound Vib. 1995;187(5):825–839.
[20] Wu TX, Thompson DJ. A hybrid model for the noise generation due to railway wheel flats. J Sound Vib. 2002;251(1):115–139.
[21] Nielsen JCO. High-frequency vertical wheel–rail contact forces – validation of a prediction model by field testing. Wear. 2008;265:1465–1471.
[22] Nielsen JCO, Lombaert G, François S. A hybrid model for prediction of ground-borne vibration due to discrete wheel/rail irregularities. J Sound Vib. 2015;345:103–120.
[23] Nielsen JCO, Kabo E, Ekberg A. Alarm limits for wheel–rail impact loads – rail bending moments generated by wheel flats. Department of Applied Mechanics, Chalmers University of Technology, Gothenburg, Sweden, 2009, 35 pp (Research report 2009:02).
[24] Newton SG, Clark RA. An investigation into the dynamic effects on track of wheelflats on railway vehicles. J Mech Eng Sci. 1979;21(4):287–297.
[25] Snyder T, Stone DH, Kristan J. Wheel flat and out-of-round formation and growth. Proceedings 2003 IEEE/ASME Joint Rail Conference; 2003; Chicago (IL), USA. p 143–148.
[26] Pieringer A, Kropp W, Nielsen JCO. The influence of contact modelling on simulated wheel/rail interaction due to wheel flats. Wear. 2014;314:273–281.
[27] Kalker JJ. Three-dimensional elastic bodies in rolling contact. Dordrecht: Kluwer Academic Publishers; 1990.
[28] Ford RAJ, Thompson DJ. Simplified contact filters in wheel/rail noise prediction. J Sound Vib. 2006;293:807–818.
[29] Hertz H. Über die Berührung fester elastischer Körper. Journal für reine und angewandte Mathematik. 1882;92:156–171.
[30] EN13674-1:2011. Railway applications – track – rail – part 1: vignole railway rails 46 kg/m and above.
[31] Wood SN. Thin plate regression splines. J. R. Statist Soc B. 2003;65(Part 1):95–114.
[32] MATLAB Release. The MathWorks. Natick MA, USA: Inc; 2015b.
[33] Fasshauer GE. Meshfree approximation methods within Matlab. In: Interdisciplinary Mathematical Sciences – vol. 6. New Jersey: World Scientific Publishing; 2007.

Appendix

The input data to the track model in Section 4 have been adopted from [21]. The discretely supported UIC60 rail is modelled by undamped Rayleigh–Timoshenko beam finite elements with bending stiffness EI = 6.4 MNm^2, shear stiffness kGA = 250 MN, mass per unit beam length m= 60 kg/m and rotational inertia per unit beam length mr^2 = 0.24 kgm. The (half) sleepers are treated as rigid with mass M_s = 150 kg. Each rail pad is modelled by a Kelvin model with discrete spring stiffness k_p = 120 kN/mm and viscous damping c_p = 25 kNs/m. The side length L_p of the pad is 0.15 m leading to rotational stiffness and damping $k_pL_p^2/12$ and $c_pL_p^2/12$, respectively. The support below each sleeper is also modelled by a Kelvin model with discrete spring stiffness k_b = 100 kN/mm

and viscous damping c_b = 82 kNs/m. The length of the track model is 70 sleeper bays with sleeper spacing$L$= 0.60 m and clamped boundaries at the two rail ends.

The coefficients in Eq (12), with flat depth d given in [mm], are: $\alpha_1 = 4.84{\cdot}10^2$, $\alpha_2 = -7.28{\cdot}10^2$, $\alpha_3 = 5.72{\cdot}10^2$, $\alpha_4 = -2.43{\cdot}10^2$, $\alpha_5 = 5.98{\cdot}10^1$, $\alpha_6 = -8.57$, $\alpha_7 = 6.74{\cdot}10^{-1}$, $\alpha_8 = -2.38{\cdot}10^{-2}$, $\alpha_9 = 1.44{\cdot}10^{-4}$. Note that the spline is only valid for $0 \leq d \leq 7$ mm as it has only been calibrated for flat depths in this interval.